CALPHAD: Computer Coupling of Phase Diagrams and Thermochemistry 39 (2012) 37–46

Contents lists available at SciVerse ScienceDirect

CALPHAD: Computer Coupling of Phase Diagrams and Thermochemistry

journal homepage: www.elsevier.com/locate/calphad

A thermodynamic assessment of the Bi–Mg–Sn ternary system

Chunju Niu, Changrong Li*, Zhenmin Du, Cuiping Guo, Sicheng Chen

School of Materials Science and Engineering, University of Science and Technology Beijing, Beijing 100083, China

ARTICLE INFO

Article history:
Received 4 June 2012
Received in revised form
18 August 2012
Accepted 30 August 2012
Available online 12 September 2012

Keywords:
The Bi–Mg–Sn ternary system
CALPHAD technique
Thermodynamic assessment
Mg-based alloys

ABSTRACT

A complete thermodynamic description of the Bi–Mg–Sn ternary system was obtained by means of the CALPHAD (CALculation of PHAse Diagram) technique. The solution phases, Rhomb, Bct_A5 and Hcp_A3, are modeled with Redlich–Kister equation. The associate model has been used to describe the liquid phase with the constituents of the species Bi, Bi_2Mg_3, Mg, Mg_2Sn and Sn. The non-stoichiometric compounds Mg_2Sn and α-Bi_2Mg_3 as well as its high temperature variant β-Bi_2Mg_3 were described by the sublattice models $(Bi,Mg)_2(Bi,Sn)_1$, $(Bi,Sn,Va)_2Mg_3$ and $(Bi,Sn)_1(Bi,Sn,Va)_3Mg_6$, respectively. The Bi–Mg–Sn ternary system has been modeled thermodynamically for the first time and the calculated phase equilibrium relations and thermochemical properties are consistent with the experimental results available in literatures.

1. Introduction

Magnesium, one of the most promising lightweight materials, is frequently used in automotive interior and other room or near-room temperature applications in the past decade [1]. The combination of high strength and low density properties is the superiority of Mg-based alloys [1–3]. Attempts have been made to develop new magnesium alloys having improved structural stability at the elevated temperatures. Recently, Mg–Sn based alloys have aroused many concerns [4–6]. Mg–Sn based alloys show some positive characteristics in terms of potential creep resistance because of the formation of stable phase Mg_2Sn, which typically distributes along the grain boundaries in as-cast Mg–Sn alloy [7,8]. However, the limited high strength and creep resistance at elevated temperatures restrict the use of magnesium alloys to applications at low temperatures [1,9]. Alloying element Bi can improve the creep resistance at all temperature. The main reason is the favorable formation of the more thermally stable Bi_2Mg_3 intermetallic compound, the reduction in the volume fraction of the less stable Mg_2Sn, and the dissolution of Bi in the remaining Mg_2Sn particles [10,11].

It is important to understand the thermodynamics of the Bi–Mg–Sn ternary system for the development of Bi-containing Mg–Sn based magnesium alloys. In order to be integrated with the substitutional/compound-energy model used in most of the Mg-based alloy systems, the Bi–Mg binary system was re-assessed in our work [12]. The aim of the present study is to obtain a consistent and reliable thermodynamic description of the Bi–Mg–Sn system in combination with the previous assessments of the Bi–Sn and the Mg–Sn binary systems reported in literatures and the Bi–Mg binary system re-optimized by present authors.

2. Experimental data on phase equilibria in the Bi–Mg–Sn system

An extensive study of the Bi–Mg–Sn system was presented by Wobst [13] who investigated the entire concentration range using thermal analysis and microscopy. The isothermal section of the Bi–Mg–Sn system at 100 °C was determined and at this temperature only α-Bi_2Mg_3 has a significant homogeneity. Four vertical sections, Bi_2Mg_3–Mg_2Sn, Bi_2Mg_3–Sn, from Bi_2Mg_3 to Sn–27.47 at% Bi (Sn–40 wt% Bi) and from Bi_2Mg_3 to Mg–38.06 at% Sn (Mg–75 wt% Sn), were measured. The invariant reactions and the liquidus projection for the Bi–Mg–Sn system were established. No ternary compound was found in the Bi–Mg–Sn system.

3. Summary of the calculated binary systems

To obtain a thermodynamic description of a muti-component system, the thermodynamic description of each low-order system is necessary. The Bi–Mg–Sn ternary system is composed of three binary sub-systems: the Bi–Mg, the Bi–Sn and the Mg–Sn systems. The evaluation results of the thermodynamic descriptions of these binary systems are summarized as follows.

3.1. The Bi–Mg binary system

The Bi–Mg binary system had been assessed by adopting the ionic melt [14] and the modified quasi-chemical models [15] to

* Corresponding author.
E-mail address: crli@mater.ustb.edu.cn (C. Li).

0364-5916/$ - see front matter © 2012 Elsevier Ltd. All rights reserved.
http://dx.doi.org/10.1016/j.calphad.2012.08.003

describe the liquid phase for its short range ordering behavior. In order to develop the thermodynamic database of the multi-component Mg-based alloys and to keep the model consistency of the related phases, the Gibbs energy descriptions of all the phases in the Bi–Mg binary system were reasonably re-modeled and critically re-assessed in our work [12]. Especially for the liquid phase, the associate model was used with the constituent species Bi, Bi_2Mg_3 and Mg. A set of self-consistent thermodynamic parameters of the Bi–Mg system was obtained and the theoretical calculations can reproduce the experimental thermochemical and phase equilibrium data well. Fig. 1 shows the calculated phase diagram of the Bi–Mg binary system with the comparison to the literature reported results [14,15].

3.2. The Bi–Sn binary system

The thermodynamic modeling of the Bi–Sn system was carried out firstly by Ohtani and Ishida [16] and Lee et al. [17]. Later, some new thermodynamic data measured by Asryan and Mikula [18] and the phase equilibria data published by Braga et al. [19] were reported. Therefore, the Bi–Sn system was re-optimized recently by Vizdal et al. [20] and Li et al. [21]. Vizdal et al. [20] adopted the substitutional solution model to describe the liquid and the two terminal solid solution phase Bct_A5 and Rhomb, and obtained a set of self-consistent thermodynamic parameters on the basis of an overall consideration of thermodynamic data and phase equilibria data, while Li et al. [21] only considered the thermodynamic data [18] and revised the interaction parameters of liquid phase on the basis of the thermodynamic parameters reported by Ohtani and Ishida [16]. Therefore, the parameters reported by Vizdal et al. [20] were adopted in the present work. The calculated Bi–Sn binary phase diagram is shown in Fig. 2.

3.3. The Mg–Sn binary system

The thermodynamic modeling and its revised dataset of the Mg–Sn system was reported in Refs. [22,23], respectively. According to Ref. [24], the inadvertent stability of the Mg-rich terminal solution Hcp_A3 phase was not noticed in Ref. [22], which is stable in the Sn-rich side in the original publication, and the complete thermodynamic parameters of all condensed phases were not published in Ref. [23]. In addition, the new experimental

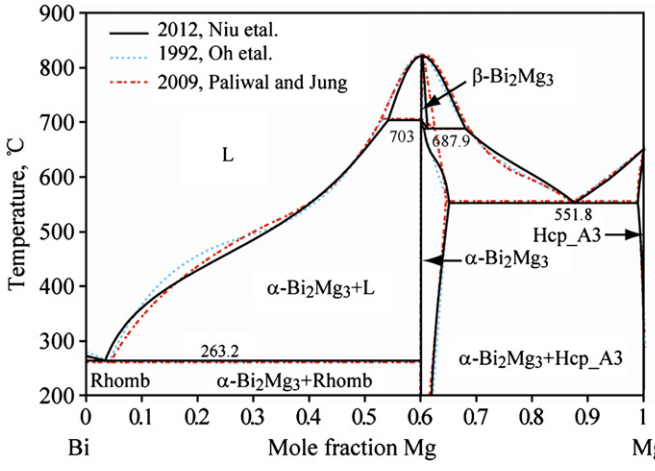

Fig. 1. Calculated phase diagram of the Bi–Mg system by Niu et al. [12] with comparison to the literature reported results [14,15].

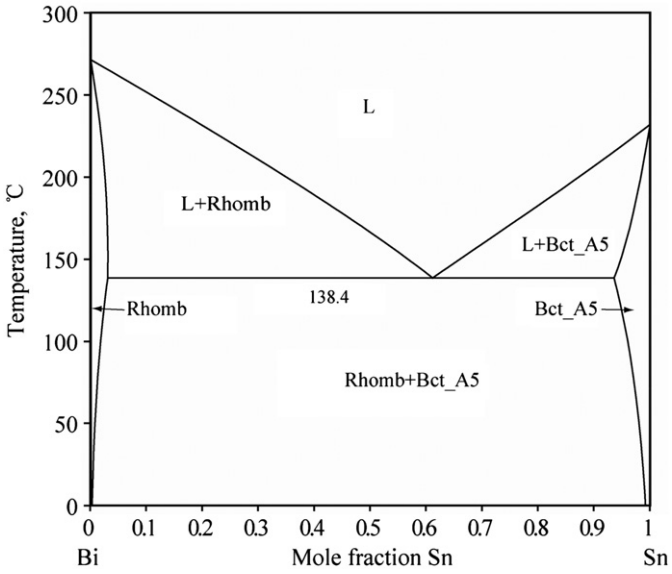

Fig. 2. Calculated phase diagram of the Bi–Sn system by Vizdal et al. [20].

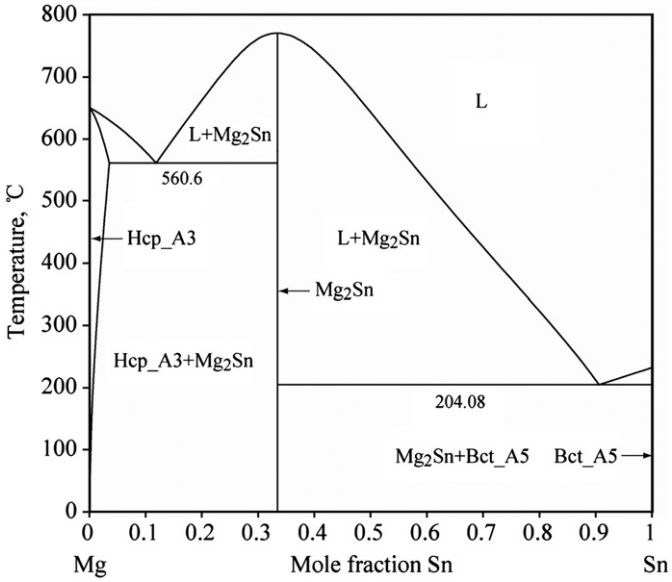

Fig. 3. Calculated phase diagram of the Mg–Sn system by Meng et al. [24].

data on the heat capacity and heat content of Mg_2Sn at low temperature were reported recently. Meng et al. [24] carried out a re-assessment for this binary system based on the comprehensive consideration and the liquid phase was described using the associate model. Therefore, the parameters of the Mg–Sn binary system provided by Meng et al. [24] were used in the present work. The calculated Mg–Sn binary phase diagram is shown in Fig. 3.

4. Thermodynamic models

4.1. Pure elements

The Gibbs energy function ${}^0G_i^{\phi}(T) = G_i^{\phi}(T) - H_i^{SER}(T)(298.15\ \mathrm{K})$ for the element i (i=Bi, Mg and Sn) in the phase ϕ (ϕ=Liq,

Table 1
Thermodynamic parameters of the Bi–Mg–Sn ternary system.

Phase, sublattice model	Thermodynamic parameters[a]	Reference
Liquid (Bi, Bi_2Mg_3, Mg, Mg_2Sn, Sn)	${}^0G^L_{Bi_2Mg_3} = -110{,}200+3T-2.9T\mathrm{Ln}T+2{}^0G^L_{Bi}+3{}^0G^L_{Mg}$	[12]
	${}^0G^L_{Bi,Bi_2Mg_3} = -36{,}000$	[12]
	${}^1G^L_{Bi,Bi_2Mg_3} = +10{,}000$	[12]
	${}^0G^L_{Bi,Mg} = -42{,}939.67-13.82T$	[12]
	${}^1G^L_{Bi,Mg} = +12T$	[12]
	${}^0G^L_{Bi_2Mg_3,Mg} = -37{,}000+20T$	[12]
	${}^1G^L_{Bi_2Mg_3,Mg} = -10{,}000$	[12]
	${}^0G^L_{Bi,Sn} = +500+1.5T$	[20]
	${}^1G^L_{Bi,Sn} = -100-0.135T$	[20]
	${}^0G^L_{Mg_2Sn} = -66{,}092.9+94.809T-11.576T\mathrm{Ln}T+{}^0G^L_{Sn}+2{}^0G^L_{Mg}$	[24]
	${}^0G^L_{Mg_2Sn,Sn} = -12{,}468.2-4.815T$	[24]
	${}^0G^L_{Mg,Mg_2Sn} = +5970.6-8.744T$	[24]
	${}^0G^L_{Mg,Sn} = -30{,}841.1+0.781T$	[24]
	${}^0G^L_{Bi,Mg_2Sn} = -29{,}947.4-20T$	This work
	${}^1G^L_{Bi,Mg_2Sn} = +19{,}161$	This work
	${}^0G^L_{Bi_2Mg_3,Mg_2Sn} = -20{,}200+10T$	This work
	${}^1G^L_{Bi_2Mg_3,Mg_2Sn} = -10{,}000$	This work
	${}^1G^L_{Bi_2Mg_3,Sn} = +10{,}000$	This work
	${}^0G^L_{Bi,Mg,Sn} = {}^1G^L_{Bi,Mg,Sn} = {}^2G^L_{Bi,Mg,Sn} = -18{,}066.9+2T$	This work
Rhomb (Bi, Sn)	${}^0G^{Rhomb}_{Bi,Sn} = +19{,}720-22.6T$	[20]
	${}^1G^{Rhomb}_{Bi,Sn} = -5760+13.834T$	[20]
Bct_A5 (Bi, Sn)	${}^0G^{Bct\_A5}_{Bi,Sn} = +3500-1.038T$	[20]
	${}^1G^{Bct\_A5}_{Bi,Sn} = -3710$	[20]
Hcp_A3 (Bi, Mg, Sn)	${}^0G^{Hcp\_A3}_{Bi,Mg} = -36{,}800-18T$	[12]
	${}^0G^{Hcp\_A3}_{Mg,Sn} = -26{,}256.5+6.234T$	[24]
	${}^1G^{Hcp\_A3}_{Mg,Sn} = -31{,}895.7$	[24]
α-Bi_2Mg_3 (Bi, Sn, Va)$_2$$Mg_3$	${}^0G^{\alpha\text{-}Bi_2Mg_3}_{Bi:Mg}\,{}^0G = -172{,}400+80.83T-10T\mathrm{Ln}T+2{}^0G^{Rhomb}_{Bi}+3{}^0G^{Hcp\_A3}_{Mg}$	[12]
	${}^0G^{\alpha\text{-}Bi_2Mg_3}_{Va:Mg} = +60{,}000-17T+3{}^0G^{Hcp\_A3}_{Mg}$	[12]
	${}^0G^{\alpha\text{-}Bi_2Mg_3}_{Bi,Va:Mg} = -38{,}500+7.8T$	[12]
	${}^1G^{\alpha\text{-}Bi_2Mg_3}_{Bi,Va:Mg} = -38{,}772.7+40T$	[12]
	${}^2G^{\alpha\text{-}Bi_2Mg_3}_{Bi,Va:Mg} = +15{,}500+20T$	[12]
	${}^0G^{\alpha\text{-}Bi_2Mg_3}_{Sn:Mg} = -40{,}000-20T+2{}^0G^{Bct\_A5}_{Sn}+3{}^0G^{Hcp\_A3}_{Mg}$	This work
β-Bi_2Mg_3 (Bi,Sn)$_1$(Bi,Sn,Va)$_3$$Mg_6$	${}^0G^{\beta\text{-}Bi_2Mg_3}_{Bi:Bi:Mg} = -210{,}083-114T+4{}^0G^{Rhomb}_{Bi}+6{}^0G^{Hcp\_A3}_{Mg}$	[12]
	${}^0G^{\beta\text{-}Bi_2Mg_3}_{Bi:Va:Mg} = +43{,}728+88T+{}^0G^{Rhomb}_{Bi}+6{}^0G^{Hcp\_A3}_{Mg}$	[12]
	${}^0G^{\beta\text{-}Bi_2Mg_3}_{Bi:Bi,Va:Mg} = -173{,}000-20T$	[12]
	${}^1G^{\beta\text{-}Bi_2Mg_3}_{Bi:Bi,Va:Mg} = -5000$	[12]
	${}^0G^{\beta\text{-}Bi_2Mg_3}_{Bi:Sn:Mg} = +62{,}074-45T+{}^0G^{Rhomb}_{Bi}+3{}^0G^{Bct\_A5}_{Sn}+6{}^0G^{Hcp\_A3}_{Mg}$	This work
	${}^0G^{\beta\text{-}Bi_2Mg_3}_{Sn:Bi:Mg} = -39{,}310.4-119.6T+3{}^0G^{Rhomb}_{Bi}+{}^0G^{Bct\_A5}_{Sn}+6{}^0G^{Hcp\_A3}_{Mg}$	This work
	${}^0G^{\beta\text{-}Bi_2Mg_3}_{Sn:Va:Mg} = -41{,}346.7+19T+{}^0G^{Bct\_A5}_{Sn}+6{}^0G^{Hcp\_A3}_{Mg}$	This work
	${}^0G^{\beta\text{-}Bi_2Mg_3}_{Sn:Sn:Mg} = -10{,}000-180T+4{}^0G^{Bct\_A5}_{Sn}+6{}^0G^{Hcp\_A3}_{Mg}$	This work
	${}^0G^{\beta\text{-}Bi_2Mg_3}_{Bi,Sn:Bi:Mg} = {}^0G^{\beta\text{-}Bi_2Mg_3}_{Bi,Sn:Sn:Mg} = {}^0G^{\beta\text{-}Bi_2Mg_3}_{Bi,Sn:Va:Mg} = -116{,}075-35T$	This work
	${}^1G^{\beta\text{-}Bi_2Mg_3}_{Bi,Sn:Bi:Mg} = {}^1G^{\beta\text{-}Bi_2Mg_3}_{Bi,Sn:Sn:Mg} = {}^1G^{\beta\text{-}Bi_2Mg_3}_{Bi,Sn:Va:Mg} = -8000+20T$	This work
	${}^0G^{\beta\text{-}Bi_2Mg_3}_{Bi:Bi,Sn:Mg} = {}^0G^{\beta\text{-}Bi_2Mg_3}_{Sn:Bi,Sn:Mg} = -120{,}288-80T$	This work
	${}^1G^{\beta\text{-}Bi_2Mg_3}_{Bi:Bi,Sn:Mg} = {}^1G^{\beta\text{-}Bi_2Mg_3}_{Sn:Bi,Sn:Mg} = -20{,}000$	This work
	${}^0G^{\beta\text{-}Bi_2Mg_3}_{Bi:Sn,Va:Mg} = {}^0G^{\beta\text{-}Bi_2Mg_3}_{Sn:Sn,Va:Mg} = -170{,}000-20T$	This work
	${}^0G^{\beta\text{-}Bi_2Mg_3}_{Sn:Bi,Va:Mg} = -173{,}000-20T$	This work
	${}^1G^{\beta\text{-}Bi_2Mg_3}_{Sn:Bi,Va:Mg} = -5000$	This work

Table 1 (*continued*)

Phase, sublattice model	Thermodynamic parameters[a]	Reference
Mg_2Sn (Bi,Mg)$_2$(Bi,Sn)	${}^0G^{Mg_2Sn}_{Mg:Sn} = -96{,}165.9+339.999T-66.285T\ln(T) -0.0121662T^2+96{,}000T^{-1}+3.33828\times10^{-7}T^3$	[24]
	${}^0G^{Mg_2Sn}_{Bi:Bi} = +29{,}484.55-53T+3{}^0G^{Rhomb}_{Bi}$	This work
	${}^0G^{Mg_2Sn}_{Bi:Sn} = +180{,}107-75T+2{}^0G^{Rhomb}_{Bi}+{}^0G^{Bct\_A5}_{Sn}$	This work
	${}^0G^{Mg_2Sn}_{Mg:Bi} = +57{,}700-60T+{}^0G^{Rhomb}_{Bi}+2{}^0G^{Hcp\_A3}_{Mg}$	This work
	${}^0G^{Mg_2Sn}_{Bi,Mg:Bi} = {}^0G^{Mg_2Sn}_{Bi,Mg:Sn} = -35{,}000-20T$	This work
	${}^1G^{Mg_2Sn}_{Bi,Mg:Bi} = {}^1G^{Mg_2Sn}_{Bi,Mg:Sn} = +113{,}000+10T$	This work
	${}^0G^{Mg_2Sn}_{Bi:Bi,Sn} = {}^0G^{Mg_2Sn}_{Mg:Bi,Sn} = -105{,}000-20T$	This work
	${}^1G^{Mg_2Sn}_{Bi:Bi,Sn} = {}^1G^{Mg_2Sn}_{Mg:Bi,Sn} = -46{,}420.5-7T$	This work

[a] Gibbs energies are expressed in J/mol. All lattice stabilities of Bi, Mg and Sn are given by Dinsdale [25].

Table 2
Invariant reactions in the Bi–Mg–Sn ternary system.

Invariant reaction	Type	T (°C)	Composition (wt%)		Reference
			w^{Liq}_{Bi}	w^{Liq}_{Mg}	
L↔β-Bi_2Mg_3+Mg_2Sn	e_2	700.6	0.555	0.200	This work
		704	0.543	0.200	[13]
β-Bi_2Mg_3↔α-Bi_2Mg_3+Mg_2Sn	e_4	659.7			This work
		656			[13]
L↔α-Bi_2Mg_3+Bct_A5	e_8	223.5	0.025	0.004	This work
		218	0.04	0.007	[13]
β-Bi_2Mg_3↔L+α-Bi_2Mg_3+Mg_2Sn	E_1	658.8	0.513	0.175	This work
		657	0.503	0.172	[13]
β-Bi_2Mg_3↔L+α-Bi_2Mg_3+Mg_2Sn	E_2	635.6	0.605	0.233	This work
		636	0.590	0.240	[13]
L↔α-Bi_2Mg_3+Hcp_A3+Mg_2Sn	E_3	522.5	0.378	0.436	This work
		522	0.390	0.437	[13]
L↔α-Bi_2Mg_3+Mg_2Sn+Bct_A5	E_4	204.05	0.002	0.021	This work
		203	0	0.021	[13]
L↔α-Bi_2Mg_3+Rhomb+Bct_A5	E_5	137.6	0.534	0.001	This work
		139	0.57	0	[13]

Rhomb, Hcp_A3 and Bct_A5) was described by the equation:

$$ {}^0G^{\phi}_i(T) = G^{\phi}_i(T) - H^{SER}_i(298.15\ \mathrm{K}) = a+bT+cT\ln(T) + dT^2+eT^3+fT^{-1}+gT^7+hT^{-9} \quad (1) $$

where $H^{SER}_i(298.15\ \mathrm{K})$ is the molar enthalpy of the stable element reference (Rhomb, Hcp_A3 and Bct_A5 for Bi, Mg and Sn, respectively) at 101,325 Pa and 25 °C, T is the absolute temperature, and a–h are coefficients. The Gibbs energy functions of the pure elements in the stable phases were taken from the SGTE compilation by Dinsdale [25] in the present work.

The Gibbs energy functions of the pure elements of the Bi–Mg and the Mg–Sn binaries [12,24] were taken from Dinsdale [25], while those of the Bi–Sn binary [20] were from the version 4.4 of the SGTE database [26]. Actually, the data of the pure Bi and Sn of Ref. [26] are the same as those of Ref. [25] from which therefore the data were adopted in the present work.

4.2. Liquid and solution phases

4.2.1. Liquid phase

The compatibility of the thermodynamic models of each low-order system is the key to the construction of multi-component database. The modified quasi-chemical models, the associate model, the ionic melt model and the substitutional model are frequently used to describe the liquid phase in numerous assessment works. The first two models are mainly used to describe the liquid phase with the short-range ordering behavior. However, the associate model is possible to be integrated with the substitutional model, which was used to describe the liquid phase for most of the Mg-based alloy systems.

In the Bi–Mg binary system [12] and the Mg–Sn binary system [24], the associate model was used to describe the liquid phase. In the Bi–Mg–Sn ternary system, the associate model was accordingly adopted with five constitute species: Bi, Bi_2Mg_3, Mg, Mg_2Sn and Sn, among which Bi_2Mg_3 and Mg_2Sn are the associated clusters. The detailed description of the associate model can be found in Refs. [27–29]. The molar Gibbs energy of the liquid phase is as follows:

$$ G^L_m(T) - H^{SER}(298.15\ \mathrm{K}) = \sum_i x_i {}^0G^L_i(T) + RT\sum_i x_i \ln x_i + {}^EG^L_m \quad (2) $$

where x_i and ${}^0G^L_i(T)$ (i=Bi, Bi_2Mg_3, Mg, Mg_2Sn and Sn) are the mole fraction and the molar Gibbs energy of the pure species i in the liquid state and ${}^EG^L_m$ is the excess Gibbs energy. ${}^0G^L_{Bi_2Mg_3}$, ${}^0G^L_{Mg_2Sn}$ and ${}^EG^L_m$ can be described by the following expressions, respectively:

$$ {}^0G^L_{Bi_2Mg_3} = a_0+b_0T+c_0T\ln T+2{}^0G^L_{Bi}+3{}^0G^L_{Mg} \quad (3) $$

$$ G^L_{Mg_2Sn} = a_1+b_1T+c_1T\ln T+2{}^0G^L_{Mg}+{}^0G^L_{Sn} \quad (4) $$

$$ {}^EG^L_m = \sum_i\sum_{j>i} x_ix_j \sum_{v=0}^{n} {}^vL^L_{i,j}(x_i-x_j)^v + \sum_i\sum_{j>i}\sum_{k>j} x_ix_jx_k(x_i{}^0L^L_{i,j,k} + x_j{}^1L^L_{i,j,k} + x_k{}^2L^L_{i,j,k}) \quad (5) $$

where, ${}^vL^L_{i,j}$ (v=0, 1, 2 and i, j=Bi, Bi_2Mg_3, Mg, Mg_2Sn and Sn) is the vth interaction parameter between the species i and j, and ${}^vL^L_{i,j,k}$ (v=0, 1, 2 and i, j, k=Bi, Bi_2Mg_3, Mg, Mg_2Sn and Sn) the interaction parameter among the species i, j and k. For the ternary interaction parameters, only ${}^0L^L_{Bi,Mg,Sn} = {}^1L^L_{Bi,Mg,Sn} = {}^2L^L_{Bi,Mg,Sn}$ is considered in the present optimization and other interaction parameters among three species are set to be zero. The interaction parameters ${}^vL^L_{i,j}$ and ${}^vL^L_{i,j,k}$

can be expressed as the linear function of temperature $a+bT$ with the coefficients a and b to be optimized.

4.2.2. Solution phases

The substitutional solution model was chosen to describe the solid solution phases, Rhomb(Bi), Hcp_A3(Mg) and Bct_A5(Sn). The expression of the molar Gibbs energy of each phase is similar with that of the liquid phase except for the contribution of the associates.

4.3. Intermetallic compounds

Three intermetallic compounds, starting from α-Bi_2Mg_3 and β-Bi_2Mg_3 in the Bi–Mg system and Mg_2Sn in the Mg–Sn system, are found in the Bi–Mg–Sn ternary system. Their Gibbs energies are described by different models as follows.

4.3.1. α-Bi_2Mg_3 phase

The intermetallic compound α-Bi_2Mg_3 in the Bi–Mg system has a homogeneity range and is described by two sublattices $(Bi,Va)_2Mg_3$ [12]. Since Mg is hardly mixed with Bi or Sn to form terminal solid solutions as shown in Fig. 1 of the Bi–Mg system and Fig. 3 of the Mg–Sn system, the intermetallic compound α-Bi_2Mg_3 of the Bi–Mg–Sn ternary system is treated as $(Bi,Sn,Va)_2Mg_3$ with some Bi atoms substituted by Sn atoms in the first sublattice. The Gibbs energy per mole of formula unit α-Bi_2Mg_3 is expressed as the following:

$$G_m^{\alpha\text{-}Bi_2Mg_3}=\sum_i y_i {}^0G_{i:Mg}^{\alpha\text{-}Bi_2Mg_3}+2RT\sum_i y_i\ln y_i$$
$$+\sum_{i1}\sum_{i2>i1} y_{i1}y_{i2}\sum_{v=0}^{n} {}^vL_{i1,i2:Mg}^{\alpha\text{-}Bi_2Mg_3}(y_{i1}-y_{i2})^v$$
$$+y_{Bi}y_{Sn}y_{Va}\left(y_{Bi}\,{}^0L_{Bi,Sn,Va:Mg}^{\alpha\text{-}Bi_2Mg_3}+y_{Sn}\,{}^1L_{Bi,Sn,Va:Mg}^{\alpha\text{-}Bi_2Mg_3}\right.$$
$$\left.+y_{Va}\,{}^2L_{Bi,Sn,Va:Mg}^{\alpha\text{-}Bi_2Mg_3}\right) \quad (6)$$

where y_i, y_{i1} and y_{i2} are the site fractions of components (i, $i1$, $i2$=Bi, Sn, Va) on the first sublattice; ${}^0G_{i:Mg}^{\alpha\text{-}Bi_2Mg_3}$ represents the Gibbs energy of the hypothetical compound i_2Mg_3 in the crystallographic structure corresponding to the α-Bi_2Mg_3 phase when the first sublattice is occupied only by the element i, relative to SER state, i.e. Rhomb for Bi, Hcp_A3 for Mg and Bct_A5 for Sn; ${}^vL_{i1,i2:Mg}^{\alpha\text{-}Bi_2Mg_3}$ represents the vth interaction parameter between the elements $i1$ and $i2$ in the first sublattice; ${}^0L_{Bi,Sn,Va:Mg}^{\alpha\text{-}Bi_2Mg_3}$, ${}^1L_{Bi,Sn,Va:Mg}^{\alpha\text{-}Bi_2Mg_3}$ and ${}^2L_{Bi,Sn,Va:Mg}^{\alpha\text{-}Bi_2Mg_3}$ are the ternary interaction parameters.

4.3.2. β-Bi_2Mg_3 phase

The intermetallic compound β-Bi_2Mg_3 phase in the Bi–Mg system also has a homogeneity range and was described by three-sublattices $(Bi)_1(Bi,Va)_3Mg_6$ [12]. Due to the similar consideration that Mg is hardly mixed with Bi or Sn as in α-Bi_2Mg_3, β-Bi_2Mg_3 in the Bi–Mg–Sn ternary system is treated as $(Bi,Sn)_1(Bi,Sn,Va)_3Mg_6$ with some Bi atoms substituted by Sn atoms in the first and the second sublattices. The Gibbs energy per mole of formula unit of $(Bi,Sn)_1(Bi,Sn,Va)_3Mg_6$ (two times of β-Bi_2Mg_3) is expressed as the following:

$$G_m^{\beta\text{-}Bi_2Mg_3}=\sum_i\sum_j y_i'y_j''\,{}^0G_{i:j:Mg}^{\beta\text{-}Bi_2Mg_3}+RT\sum_i y_i'\ln y_i'+3RT\sum_j y_j''\ln y_j''$$

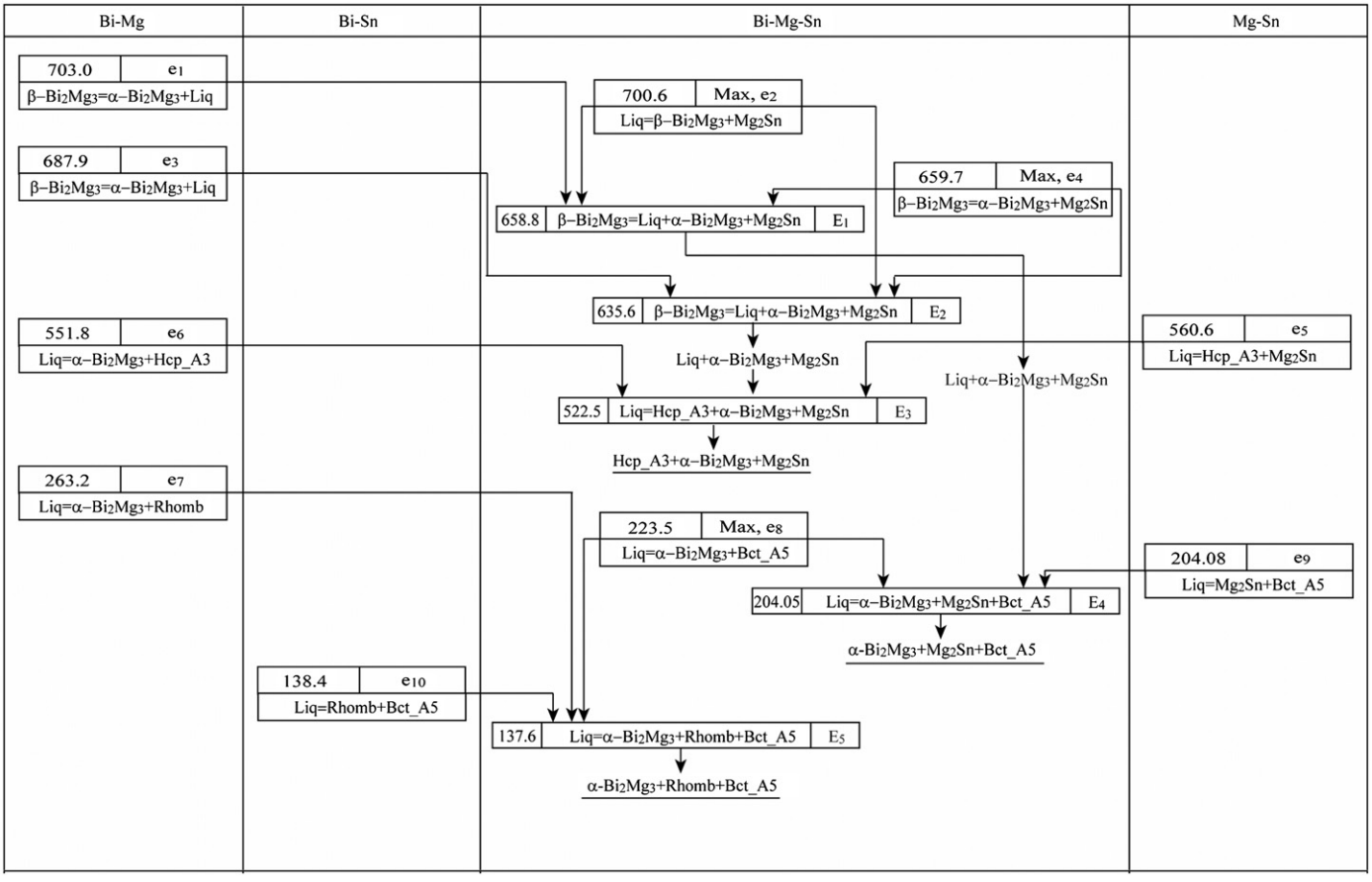

Fig. 4. Reaction scheme of the Bi–Mg–Sn ternary system (temperature,°C).

$$+\sum_i y'_i\left(\sum_{j1}\sum_{j2>j1} y''_{j1}y''_{j2}\sum_{v=0}^{n} {}^{v}L^{\beta\text{-}Bi_2Mg_3}_{i:j1,j2:Mg}(y''_{j1}-y''_{j2})^v\right)$$
$$+\sum_j y''_j\left(\sum_{i1}\sum_{i2>i1} y'_{i1}y'_{i2}\sum_{v=0}^{n} {}^{v}L^{\beta\text{-}Bi_2Mg_3}_{i1,i2:j:Mg}(y'_{i1}-y'_{i2})^v\right) \quad (7)$$

where y'_i, y'_{i1}, y'_{i2}, y''_j, y''_{j1} and y''_{j2} are the site fractions of the components i, $i1$, $i2$, j, $j1$ and $j2$ (i, $i1$, $i2$=Bi, Sn and j, $j1$, $j2$=Bi, Sn, Va), respectively; ${}^{0}G^{\beta\text{-}Bi_2Mg_3}_{i:j:Mg}$ is the Gibbs energy of the hypothetical compound $i_1j_3Mg_6$; ${}^{v}L^{\beta\text{-}Bi_2Mg_3}_{i1,i2:j:Mg}$ and ${}^{v}L^{\beta\text{-}Bi_2Mg_3}_{i:j1,j2:Mg}$ are the interaction parameters between $i1$ and $i2$ in the first sublattice and between $j1$ and $j2$ in the second sublattice, respectively. The binary thermodynamic parameters for the Bi–Mg terminal intermetallic compound of the β-Bi_2Mg_3 ternary phase have been assessed by Niu et al. [12] and the other parameters need to be assessed in the present work.

4.3.3. Mg_2Sn phase

The Mg_2Sn phase in the Mg–Sn binary system is a stoichiometric intermetallic compound. In the Bi_2Mg_3–Mg_2Sn vertical section, the maximum solubility of Bi in the Mg_2Sn phase of the Bi–Mg–Sn ternary system is 8.13 at% (26.40 wt%) at 704 °C [13]. The extension of the model of the Mg_2Sn is governed by the crystallography of the phase and the capability of Bi to occupy various sublattice positions. Since the crystallographic structure of Mg_2Sn is of the CaF_2 prototype with two sublattice occupations, Mg (8c) at (1/4, 1/4, 1/4) and Sn (4a) at (0, 0, 0), the Bi atoms may be supposed to substitute the atoms in either sublattice to form a certain amount of solubility. If the Bi atoms get into only one of the two sublattices, the solubility of Bi in Mg_2Sn cannot be observed in the Bi_2Mg_3–Mg_2Sn vertical section. Therefore, the ternary Mg_2Sn phase was treated as $(Bi,Mg)_2(Bi,Sn)_1$ in the present work. The Gibbs energy per mole of the formula unit Mg_2Sn is expressed as the following:

$$G^{Mg_2Sn}_m=\sum_i\sum_j y'_iy''_j{}^{0}G^{Mg_2Sn}_{i:j}+2RT\sum_i y'_i\ln y'_i+RT\sum_j y''_j\ln y''_j$$
$$+\sum_i y'_iy''_{Bi}y''_{Sn}\sum_{v=0}^{n}{}^{v}L^{Mg_2Sn}_{i:Bi,Sn}(y''_{Bi}-y''_{Sn})^v$$
$$+\sum_j y''_jy'_{Bi}y'_{Mg}\sum_{v=0}^{n}{}^{v}L^{Mg_2Sn}_{Bi,Mg:j}(y'_{Bi}-y'_{Mg})^v \quad (8)$$

where y'_i and y''_j are the site fractions of the components i and j (i=Bi, Mg and j=Bi, Sn) in the first and the second sublattices; ${}^{0}G^{Mg_2Sn}_{i:j}$ is the Gibbs energy of the constituent compound i_2j in the crystallographic structure corresponding to the Mg_2Sn phase. Since Mg_2Sn is the real compound in the Mg–Sn binary system, ${}^{0}G^{Mg_2Sn}_{Mg:Sn}$ was optimized by Meng et al. [24]. While the other constituent compound i_2j is the hypothetical one and ${}^{0}G^{Mg_2Sn}_{i:j}$ needs to be assessed in the present work; ${}^{v}L^{\beta\text{-}Bi_2Mg_3}_{Bi,Mg:j}$ and ${}^{v}L^{\beta\text{-}Bi_2Mg_3}_{i:Bi,Sn}$ are the interaction parameters between Bi and Mg in the first sublattice and between Bi and Sn in the second sublattice, respectively.

5. Results and discussion

The optimization of thermodynamic parameters has been carried out with the help of the PARROT module of Thermo-Calc software [30] and on the basis of the evaluated experimental phase equilibria. The working strategy is the minimization of the square sum of the difference between experimental data and computed values. The thermodynamic parameters of the Bi–Mg–Sn ternary system obtained finally in the present work are summarized in Table 1. The calculated invariant reactions and the reaction scheme of the invariant reactions of the Bi–Mg–Sn system are given in Table 2 and Fig. 4, respectively. The reasonable agreement is achieved between the calculated results and the experimental data.

5.1. Isothermal section and liquidus projection

The morphologies of the calculated phase diagrams are essentially consistent with those constructed by Wobst [13], as shown in Figs. 5 and 6.

Fig. 5 is the calculated isothermal section at 100 °C as well as the comparison with the available experimental phase equilibrium data. The main difference between the calculated results based on the assessed thermodynamic parameters and the estimated diagram according to the experimental data is the existence ranges of the two-phase regions of both Rhomb+α-Bi_2Mg_3 and Bct_A5+α-Bi_2Mg_3

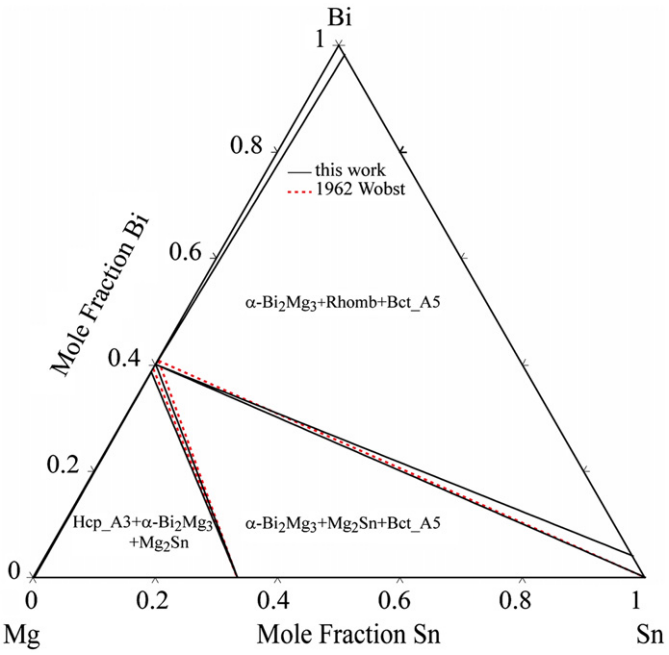

Fig. 5. Isothermal section of the Bi–Mg–Sn ternary system at 100 °C.

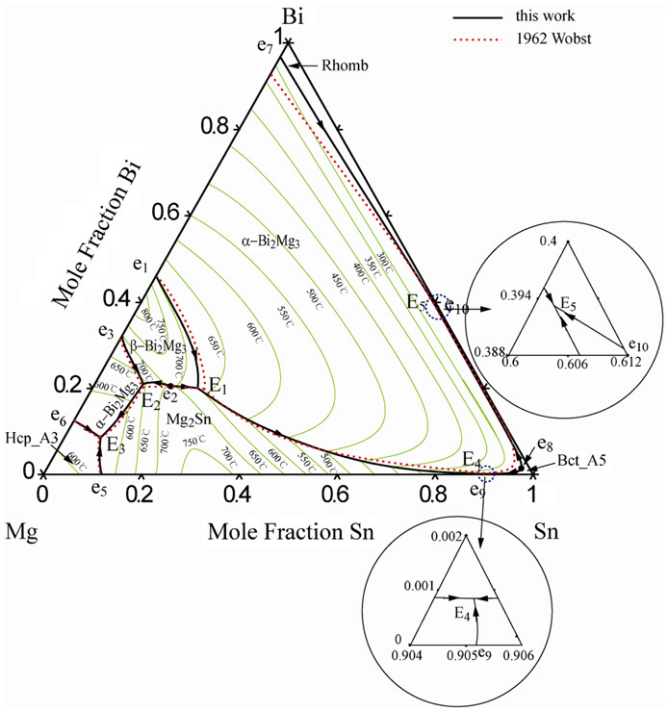

Fig. 6. Liquid projection of the Bi–Mg–Sn ternary system.

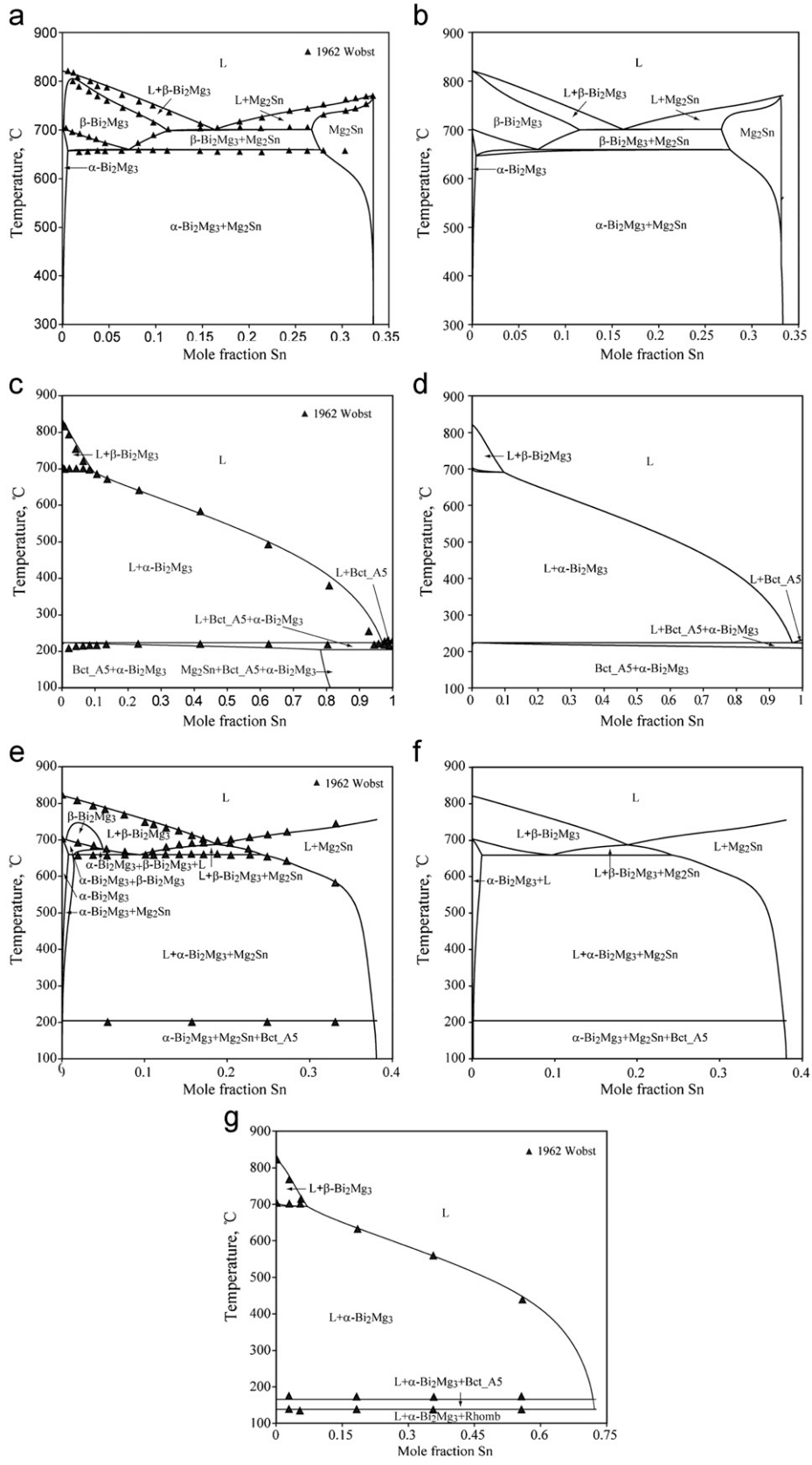

Fig. 7. Calculated vertical sections in the Bi–Mg–Sn ternary system comparison with experimental data [13]. (a) from Bi_2Mg_3 to Mg_2Sn; (b) from Bi–60.2 at% Mg to Mg_2Sn; (c) Bi_2Mg_3–Sn; (d) from Bi_2Mg_3 to Sn–0.01 at% Bi; (e) from Bi_2Mg_3 to Mg–38.06 at% Sn; (f) from Bi–59.94 at% Mg to Mg–38.06 at% Sn and (g) from Bi_2Mg_3 to Bi–72.53 at% Sn.

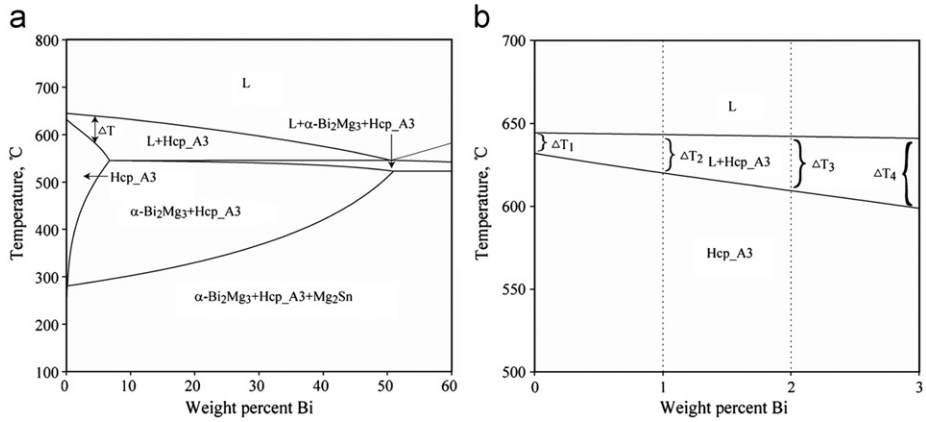

Fig. 8. Undercooling degree at different amounts of Bi in the Mg–5Sn based alloys. (a) Calculated vertical section from Mg–5Sn to Mg–5Sn–60Bi and (b) enlargement of the Mg-rich side.

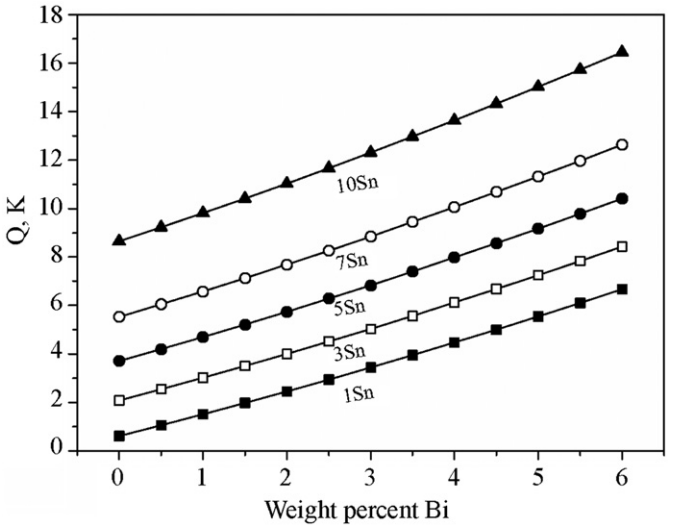

Fig. 9. Calculated values of Q in Bi–Mg–Sn alloys at constant Sn content of 1, 3, 5, 7 and 10 wt%.

and the solubility range of α-Bi_2Mg_3. With the consideration of the experimental errors, the small difference between the calculated and the experimental phase diagram can be acceptable.

The calculated liquidus projection is shown in Fig. 6. Seven primary crystallization areas are observed in this ternary system. The calculation is in well accord with the experiments reported by Wobst [13], except for the boundary of the Rhomb primary crystallization area. The main reason is the different concentrations of Bi of the liquid phase of the eutectic reaction L↔α-Bi_2Mg_3+Rhomb in the Bi–Mg binary system.

5.2. Vertical sections

Fig. 7 shows the calculated vertical sections of the Bi–Mg–Sn ternary system in comparison with the experimental information [13].

Fig. 7(a) is the Bi_2Mg_3–Mg_2Sn vertical section. Owing to the solubility ranges of the Bi_2Mg_3 (α and β) and Mg_2Sn phases and the small composition deviation of the β-Bi_2Mg_3 phase from its stoichiometry (60 at% Mg) in the terminal Bi–Mg binary system, this vertical section in Fig. 7(a) is not really a pseudo-binary diagram and the two-phase region L+β-Bi_2Mg_3 appears at the left side at high temperature. If the starting point of the x-axis of Fig. 7(a) is changed to a slightly more Mg containing composition (60.2 at% Mg) than Bi_2Mg_3 (60 at% Mg), the calculated vertical section, Fig. 7(b), exhibits more like a conventional pseudo-binary diagram with the equilibrium tie-lines very close to the plane of the section.

Fig. 7(c) and (e) shows the vertical sections from Bi_2Mg_3 to Sn and from Bi_2Mg_3 to Mg–38.06 at% Sn (Mg–75 wt% Sn), respectively, in both of which some superfluous regions exist in comparison with the experimental information. If the ending and the starting points of the x-axis in Fig. 7(c) and (e) are changed slightly, the more consistent vertical sections are obtained, as shown in Fig. 7(d) (from Bi_2Mg_3 to Sn–0.01 at% Bi) and 7(f) (from Bi–59.94 at% Mg to Mg–38.06 at% Sn).

The calculated phase boundaries of the vertical section from Bi_2Mg_3 to Bi–72.53 at% Sn, Fig. 7(g), are in good agreement with experimental data.

5.3. Simulation and analysis of solidification process

5.3.1. Degree of undercooling and growth restriction factor

Keyvani et al. [11] investigated the effect of Bi additions on the creep behavior of Mg–Sn alloys. By means of the optical micrographs of four typical alloys with 0, 1, 2 and 3 wt% Bi, the coarse dendritic structure of the as-cast Mg–5Sn alloy with 5 wt% Sn is refined generally after the addition of Bi.

Generally, when the degree of undercooling is increasing in a certain range, the nucleation rate is increasing as well and the coarse grains can be refined. Fig. 8 shows the increment of undercooling degree when the content of Bi is increasing in a certain range.

The growth restriction factor Q, $Q=(\partial\Delta T_{cs}/\partial f_s)_{fs\to 0}$, is the key quantity of the solutal effect on grain growth and grain refinement during solidification of alloys [31]. ΔT_{cs} and f_s are the constitutional undercooling degree (the difference between the liquidus temperature and the real solidification temperature, T_L-T) and the fraction of solid respectively. The grain size is of a simple linear relation with the inverse of the growth restriction factor Q [32]. Fig. 9 gives the growth restriction factor Q in the Bi–Mg–Sn alloys at constant Sn contents of 1, 3, 5, 7 and 10 wt%. The calculated value of Q increases with increasing Bi content.

In the experimental results reported by Keyvani et al. [11], the as-cast Mg–5Sn alloy is refined generally after the addition of Bi, which can be well interpreted by the increments of both the undercooling degree and the growth restriction factor as shown in Figs. 8 and 9, respectively.

5.3.2. Analysis of solidification process

The solidification paths from 750 °C of the above four representative alloys are simulated by Scheil solidification approach, as shown in Fig. 10. The calculation results are generally the same as those measured by Keyvani et al. [11]. For the alloys Mg–5Sn–xBi (x=1, 2 and 3 wt%), both the experiment and calculation show that the first solidified phase is the primary phase Hcp_A3, then the liquid composition moves to the liquid↔Hcp_A3+Mg_2Sn eutectic valley along which the two phases Hcp_A3 and Mg_2Sn which crystallize simultaneously, and at last the liquid composition moves to the four-phase invariant equilibria, Liquid↔Hcp_A3+Mg_2Sn+α-Bi_2Mg_3, at 522.54 °C at which the three phases Hcp_A3+Mg_2Sn+α-Bi_2Mg_3 crystallize simultaneously until the liquid phase disappears.

According to the literature reported by Keyvani et al. [11], adding Bi to the Mg–5Sn alloy improves its creep resistance at all temperatures. The main reason is that the formation of the less stable Mg_2Sn phase is suppressed and the volume fraction of the more thermally stable Bi_2Mg_3 increases. Fig. 11 shows the weight fractions of Bi_2Mg_3 and Mg_2Sn varying with the Bi content by the Scheil solidification approach. The calculated results, the increasing of Bi_2Mg_3 and the decreasing of Mg_2Sn with the increasing Bi content are consistent with the literature explanation [11].

6. Conclusions

The phase equilibrium relations of the Bi–Mg–Sn ternary system available in literatures were critically evaluated. The Gibbs energy

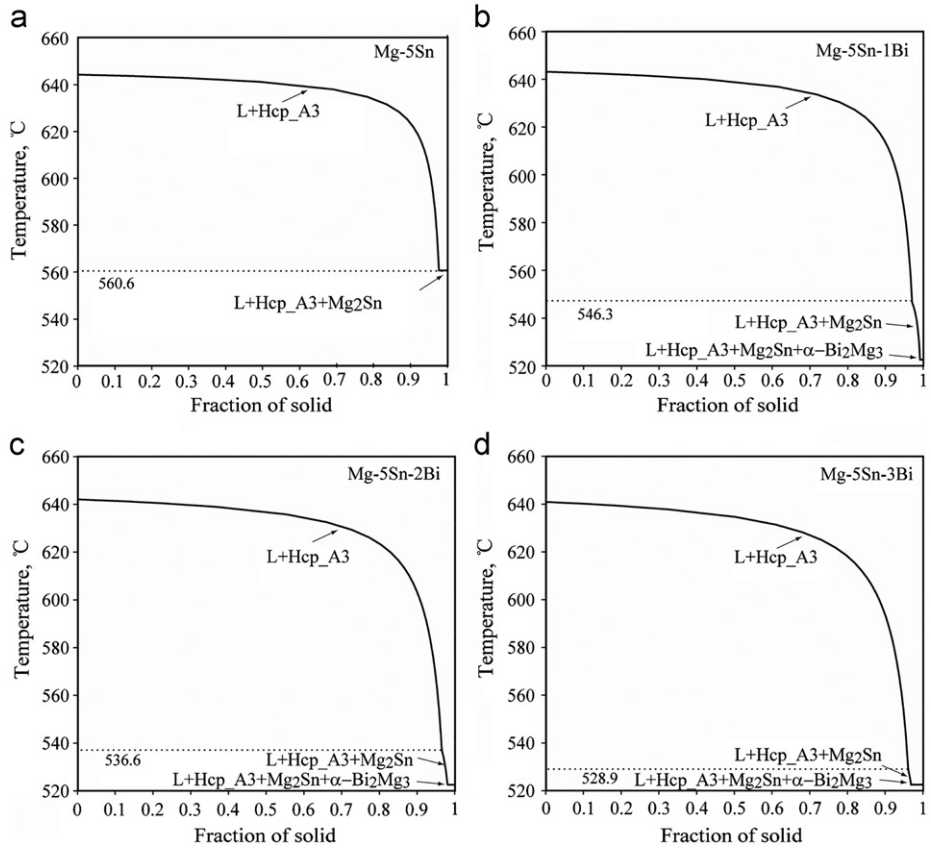

Fig. 10. Calculated solidification path for the four typical alloys. (a) Mg–5Sn alloys; (b) Mg–5Sn–1Bi alloys; (c) Mg–5Sn–2Bi alloys and (d) Mg–5Sn–3Bi alloys.

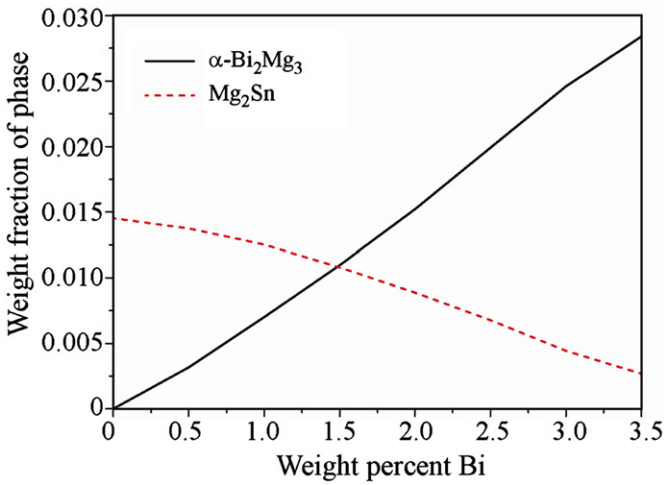

Fig. 11. Weight fraction of phase at different amounts of Bi.

descriptions of all the phases of the system were reasonably proposed. A self-consistent set of thermodynamic parameters was obtained. The CALPHAD results can reproduce the experimental phase equilibrium relations well, including the liquidus surface projection, the iso-thermal and the vertical sections. The simulation of the solidification processes of the typical alloys Mg–5Sn–*x*Bi ($x=0$, 1, 2 and 3) explains reasonably the experimental results showing the useful addition of the Bi content. The present thermodynamic assessment of the Bi–Mg–Sn ternary system is a contribution to the development of the thermodynamic database of the multi-component Mg-based alloys.

Acknowledgments

This work was supported by the National Natural Science Foundation of China (nos. 50731002 and 50671009).

Appendix A. Supporting information

Supplementary data associated with this article can be found in the online version at http://dx.doi.org/10.1016/j.calphad.2012.08.003.

References

[1] A.A. Luo, Int. Mater. Rev. 49 (1) (2004) 13–30.
[2] M.K. Kulekci, Int. J. Adv. Manuf. Technol. 39 (9) (2008) 851–865.
[3] C. Blawert, N. Hort, K.U. Kainer, Trans. Indian Inst. Met. 57 (4) (2004) 397–408.
[4] D.H. Kang, S.S. Park, Y.S. Oh, N.J. Kim, Mater. Sci. Eng. A 449–451 (2007) 318–321.
[5] N. Hort, Y. Huang, T. Abu Leil, P. Maier, K.U. Kainer, Adv. Eng. Mater. 8 (5) (2006) 359–364.
[6] H.K. Lim, D.H. Kim, J.Y. Lee, W.T. Kim, D.H. Kim, J. Alloys Compd. 468 (1–2) (2009) 308–314.
[7] S.H. Wei, Y.G. Chen, Y.B. Tang, M. Liu, S.F. Xiao, X.P. Zhang, Y.H. Zhao, Trans. Nonferrous Met. Soc. China 18 (2008) s214–s217.
[8] H.M. Liu, Y.G. Chen, Y.B. Tang, S.H. Wei, G. Niu, J. Alloys Compd. 440 (2007) 122–126.
[9] B.L. Mordike, T. Ebert, Mater. Sci. Eng. A 302 (1) (2001) 37–45.
[10] M. Keyvani., R. Mahmudi, G. Nayyeri, Mater. Sci. Eng. A 527 (2010) 7714–7718.
[11] M. Keyvani, R. Mahmudi, G. Nayyeri, Metall. Mater. Trans. A 42 (7) (2011) 1990–2003.
[12] C.J. Niu, C.R. Li, Z.M. Du, C.P. Guo, Y.J. Jing, Acta Metall. Sin. (Engl. Lett.) 25 (1) (2012) 19–28.
[13] M. Wobst, Z. Phys. Chem. 219 (1962) 239–265.

[14] C.S. Oh, S.Y. Kang, D.N. Lee, Calphad 16 (2) (1992) 181–191.
[15] M. Paliwal, I.H. Jung, Calphad 33 (4) (2009) 744–754.
[16] H. Ohtani, K. Ishida, J. Electron. Mater. 23 (8) (1994) 747–755.
[17] B.-J. Lee, C.-S. Oh, J.-H. Shim, J. Electron. Mater. 25 (6) (1996) 983–991.
[18] N. Asryan, A. Mikula, Z. Metallkd. 95 (3) (2004) 132–135.
[19] M.H. Braga, J. Vizdal, A. Kroupa, J. Ferreira, D. Soares, L.F. Malheiros, Calphad 31 (4) (2007) 468–478.
[20] J. Vizdal, M.H. Braga, A. Kroupa, K.W. Richter, D. Soares, L.F. Malheiros, J. Ferreira, Calphad 31 (4) (2007) 438–448.
[21] Z.A. Li, Z.M. Cao, S. Knott, A. Mikula, Y. Du, Z.Y. Qiao, Calphad 32 (1) (2008) 152–163.
[22] S.G. Fries, H.L. Lukas, J. Chim. Phys. 90 (2) (1993) 181–187.
[23] A. Kozlov, M. Ohno, R. Arroyave, Z.K. Liu, R. Schmid-Fetzer, Intemetallics 16 (2008) 199–315.
[24] F.G. Meng, J. Wang, L.B. Liu, Z.P. Jin, J. Alloys Compd. 508 (2010) 570–581.
[25] A.T. Dinsdale, Calphad 15 (4) (1991) 317–425.
[26] Version 4.4 of the SGTE Unary Database.
[27] F. Sommer, Z. Metallkd. 73 (2) (1982) 72–76.
[28] F. Sommer, Z. Metallkd. 73 (2) (1982) 77–86.
[29] R. Schmid, Y.A. Chang, Calphad 9 (4) (1985) 363–382.
[30] B. Sundman, B. Jansson, J.O. Andersson, Calphad 9 (2) (1985) 153–190.
[31] R. Schmid-Fetzer, A. Kozlov, Acta Mater. 59 (2011) 6133–6144.
[32] D.H. Stjon, M.A. Easton, P. Cao, M. Qian, Int. J. Cast Met. Res. 20 (3) (2007) 131–135.